AIP Journal of Applied Physics

The effect of oxide shell thickness on the structural, electronic, and optical properties of Si-SiO2 core-shell nano-crystals: A (time dependent)density functional theory study

Sanaz Nazemi, Mahdi Pourfath, Ebrahim Asl Soleimani, and Hans Kosina

Citation: Journal of Applied Physics **119**, 144302 (2016); doi: 10.1063/1.4945392
View online: http://dx.doi.org/10.1063/1.4945392
View Table of Contents: http://scitation.aip.org/content/aip/journal/jap/119/14?ver=pdfcov
Published by the AIP Publishing

The effect of oxide shell thickness on the structural, electronic, and optical properties of Si-SiO_2 core-shell nano-crystals: A (time dependent)density functional theory study

Sanaz Nazemi,[1,a)] Mahdi Pourfath,[1,2,a)] Ebrahim Asl Soleimani,[1] and Hans Kosina[2]
[1]*School of Electrical and Computer Engineering, University of Tehran, Tehran 14395-515, Iran*
[2]*Institute for Microelectronics, Technische Universität Wien, Wien A-1040, Austria*

(Received 10 January 2016; accepted 18 March 2016; published online 11 April 2016)

Due to their tunable properties, silicon nano-crystals (NC) are currently being investigated. Quantum confinement can generally be employed for size-dependent band-gap tuning at dimensions smaller than the Bohr radius (~5 nm for silicon). At the nano-meter scale, however, increased surface-to-volume ratio makes the surface effects dominant. Specifically, in Si-SiO_2 core-shell semiconductor NCs the interfacial transition layer causes peculiar electronic and optical properties, because of the co-existence of intermediate oxidation states of silicon (Si^{n+}, n = 0–4). Due to the presence of the many factors involved, a comprehensive understanding of the optical properties of these NCs has not yet been achieved. In this work, Si-SiO_2 NCs with a diameter of 1.1 nm and covered by amorphous oxide shells with thicknesses between 2.5 and 4.75 Å are comprehensively studied, employing density functional theory calculations. It is shown that with increased oxide shell thickness, the low-energy part of the optical transition spectrum of the NC is red shifted and attenuated. Moreover, the absorption coefficient is increased in the high-energy part of the spectrum which corresponds to SiO_2 transitions. Structural examinations indicate a larger compressive stress on the central silicon cluster with a thicker oxide shell. Examination of the local density of states reveals the migration of frontier molecular orbitals from the oxide shell into the silicon core with the increase of silica shell thickness. The optical and electrical properties are explained through the analysis of the density of states and the spatial distribution of silicon sub-oxide species. © *2016 AIP Publishing LLC*. [http://dx.doi.org/10.1063/1.4945392]

I. INTRODUCTION

One of the motivation for the study of silicon nanostructures is their ability for quasi-direct transitions that improves the weak phonon-assisted optical activity of silicon.[1] Furthermore, the possibility of the band-gap engineering in the strong confinement regime ($r < a_{Bohr}$)[2–5] renders silicon NC as a promising candidate for photovoltaics and optoelectronics.[6–9] Quantum confinement effects on the optical properties of silicon NCs have been studied for the first time with intense visible-light emission from porous silicon.[10] However, because of numerous inter-related parameters including interfacial stress,[11,12] defects,[13,14] suboxide species,[15–17] and the chemistry,[18–20] and geometry[21–23] of the NC's surface, the electronic and optical properties are still a subject of debate.

Chopra and Rai have studied the effect of surface passivation of silicon NCs (<1 nm) with hydrogen, fluorine, and chlorine.[24] They have reported that the surface passivation and the cluster size only weakly affect the conductivity of considered NCs. Oxygen as a widely used material in silicon technology is well known for the modification of the optical and electrical properties of silicon NCs.[8,9,20] Puzder *et al.*[25] have used quantum Monte Carlo simulations to show a significant gap reduction in fully hydrogenated NCs with only a few oxygen atoms at the surface of the NC. They have shown that a double-bonded oxygen atom reduces the optical gap more effectively than bridged ones. By increasing the number of oxygen passivants, the band-gap is further reduced.[25] The largest number of oxygen atoms exists at Si-SiO_2 interfaces, specifically in the core-shell NCs with silicon core and oxide shell which appears in some important structures including porous silicon and silicon NCs embedded in silica host.[11,14,16,17] Due to the complexity of the interface, however, few theoretical studies have been performed on silicon NCs with SiO_2 capping shell.[26–28] The first study on Si-SiO_2 core-shell NC was performed by Wolkin *et al.*[29] They have investigated the variation of photoluminescence (PL) spectra of oxygen-free porous silicon samples for progressively increased time of exposure to air. A redshift in PL spectra during the first minutes of air-exposure has been reported, without any significant variation for an air-exposure longer than 200 min. This behavior has been explained in terms of three different recombination mechanisms that depend on the size of the NC: (1) recombination via free excitons in large NCs, (2) recombination of trapped electrons with free holes in intermediate size NCs, and (3) recombination via trapped excitons in small NCs (diameters smaller than 2 nm).

For silicon NCs embedded in SiO_2 host, Liao *et al.*[30] have deconvolved the Raman peaks into three of nanocrystalline, amorphous, and the intermediate components associated with the bond dilation at the grain boundary. Arguirov *et al.*[11] have reported residual compressive stress on silicon NC embedded in SiO_2 host, which is also observed in our results for core-shell NCs. Many experimental techniques

[a)]Electronic addresses: s.nazemi@ut.ac.ir and pourfath@ut.ac.ir

have been utilized for determining the structure of Si-SiO_2 interface and its extent,[16,31] but this remains elusive despite many efforts. For flat SiO_2-Si(100) and SiO_2-Si(111) interfaces, the distribution and intensity of intermediate oxidation states of silicon have been studied using X-ray photo-electron spectroscopy (XPS) and Raman spectroscopy.[16,32–34] The experimental results range from atomically sharp to extended interfaces of about 7 Å wide consisted of a few atomic layers containing silicon sub-oxide species, while most of the structural models assume an atomically abrupt interface with an average transition region of ~2–3 Å wide.[35,36]

Zhou *et al.*[26] have presented the first *ab-initio* study on silicon-oxide interface by replacing hydrogen with hydroxyl in hydrogen passivated silicon NCs. They have shown that oxygen atoms localize the highest occupied molecular orbital (HOMO) and the lowest un-occupied molecular orbital (LUMO) which has been ascribed to the weakening of the Si-Si back-bonds at interface silicon atoms. This finding, which is also in good agreement with our results, is confirmed by later works.[20,25,37] Many studies[27,38–41] have defined the Si-SiO_2 nano-structures in the form of spherical silicon NCs embedded in β-cristobalite, polymorph of silicon dioxide, which imposes much excessive unreal stress and defects to the interface. Nama *et al.* have employed an *ab initio* restricted Hartree-Fock method along with a large unit cell to study core-shell Si-SiO_2 NCs with cubic and parallelepiped silicon core.[42] They have shown that the lattice constant of the core and oxidized surface decreases as the NC size increases. In this work, we have employed the model described in Ref. 28 which results in a smaller interface roughness. Density functional theory (DFT) calculations are used to study Si-SiO_2 core-shell nano-structures with 1.1 nm diameter silicon core and amorphous oxide shell with thicknesses in the range of 2.5–4.75 Å.

The paper is organized as follows: Sec. II describes the employed computational method, Sec. III discusses the effect of oxide shell thickness on the optical transitions of the nano structure, the structural properties of the silicon core, the partial density of states, the spatial density distributions of the frontier molecular orbitals of core-shell Si-SiO_2 NCs with 1.6, 1.8, and 2.05 nm diameters. Finally, concluding remarks are presented in Sec. IV.

II. STRUCTURES AND APPROACH

In core-shell Si-SiO_2 NCs, the effect of oxide shell can interfere with that of quantum confinement and even dominates it. Thus, the main objective of our work is elucidating the oxide-induced modifications in the electronic and optical properties of such NCs. The initial model of NCs is defined by requiring the satisfaction of the following points: (i) According to the experimental work of Matsumoto *et al.*,[43] the crystallographic planes are exposed during the fabrication process of core-shell Si-SiO_2 NC. Hence, the initial NCs are defined in the form of Wulff shapes. (ii) The exposed crystallographic planes in the core silicon and in the oxide shell are not pure crystallines.[43,44] Thus, the amorphous phase of silica is used for the capping shell. (iii) The β-cristobalite is well-known to have a simple interface with silicon compared to other polymorphs of silicon dioxide,[44,45] because of its cubic lattice. However, in this scheme the interfacial stress and defects are overestimated, specifically for our considered curved interfaces. We have utilized the method of Kroll and Schulte[28] which was proposed for silicon NCs in SiO_2 host that minimizes the dangling bonds and defects at the interface which accordingly results in a smoother interface at the glass matrix after relaxation.

We have defined NCs as Wulff shapes with 1.6, 1.8, and 2.05 nm diameters carved from bulk silicon, in the form of energy-minimized structures made from crossed crystallographic planes including the (100), (110), and (111) with relative surface energies of 1, 0.8, and 0.86, respectively.[46] The 1–3 nm size of NCs is consistent with the NC sizes defined in the literature.[15,42,47] In the next step, the oxide layer is introduced into the surface of silicon Wulffs. According to the method proposed by Kroll and Schulte,[28] amorphous silica is defined by adding oxygen atoms on the Si-Si bonds. Accordingly, we add oxygen atoms outside the central 1.1 nm diameter silicon Wulff resulting in $Si_{128}O_{115}$, $Si_{172}O_{190}$, and $Si_{274}O_{372}$ NCs with oxide shell thicknesses of 2.5, 3.5, and 4.75 Å, respectively (see Fig. 1).

The DFT calculations are carried out using the SIESTA code.[48] The generalized gradient approximation (GGA) is utilized based on the Perdew-Bruke-Ernzerhov (PBE) version of exchange-correlation functionals generated using the fhi98PP code.[49] Norm conserving pseudo-potentials along with numerical atomic orbitals with double ζ polarized basis set and a kinetic energy cutoff of 100 Ry are assumed. Vacuum is added on all sides in order to have a large enough supercell that prevents the interaction of neighboring cells. The structures are relaxed using conjugate gradient calculations until the maximum force on each atom becomes smaller than 0.02 eV/Å. The duration of structural relaxation calculations took about four months on a dual socket server with 2 × AMD Opteron 6132 (8 cores, 2.2 GHz) processors.

The considered supercells consist of 243, 362, and 646 atoms. Because of the required computational demand, the optical calculations are performed based on the first-order time-dependent perturbation theory, as implemented in the SIESTA code.[48] The optical properties are evaluated based on the complex dielectric function $\epsilon(\omega) = \epsilon_1(\omega) + i\epsilon_2(\omega)$, with the imaginary part[50]

$$\epsilon_2(\omega) = \frac{e^2\hbar}{\pi m^2\omega^2}\sum_{i,j}\int_{BZ} d\mathbf{k}|W_{ij}(\mathbf{k})|^2\delta\big(\omega - \omega_{ij}(\mathbf{k})\big), \quad (1)$$

where the sum runs over all possible pairs of states in the valence $|\phi_i\rangle$ and conduction $|\phi_j\rangle$ bands with corresponding eigenvalues E_i and E_j, such that $\hbar\omega_{ij}(\mathbf{k}) = E_i - E_j$. The electronic diploe transition matrix element $W_{ij}(\mathbf{k})$, which represents the transition rate from state $|\phi_i\rangle$ to state $|\phi_j\rangle$, is given by $W_{ij}(\mathbf{k}) = \langle\phi_j(\mathbf{k})|\hat{\mathbf{e}}\cdot\mathbf{p}|\phi_i(\mathbf{k})\rangle$, with $\hat{\mathbf{e}}$ and $\mathbf{p}$ are the polarization vector and the momentum operator, respectively. The absorption coefficient is then extracted using the Kramers-Kronig relation[51,52] which is based on the causality, linear response theory, and the boundedness of physical observables

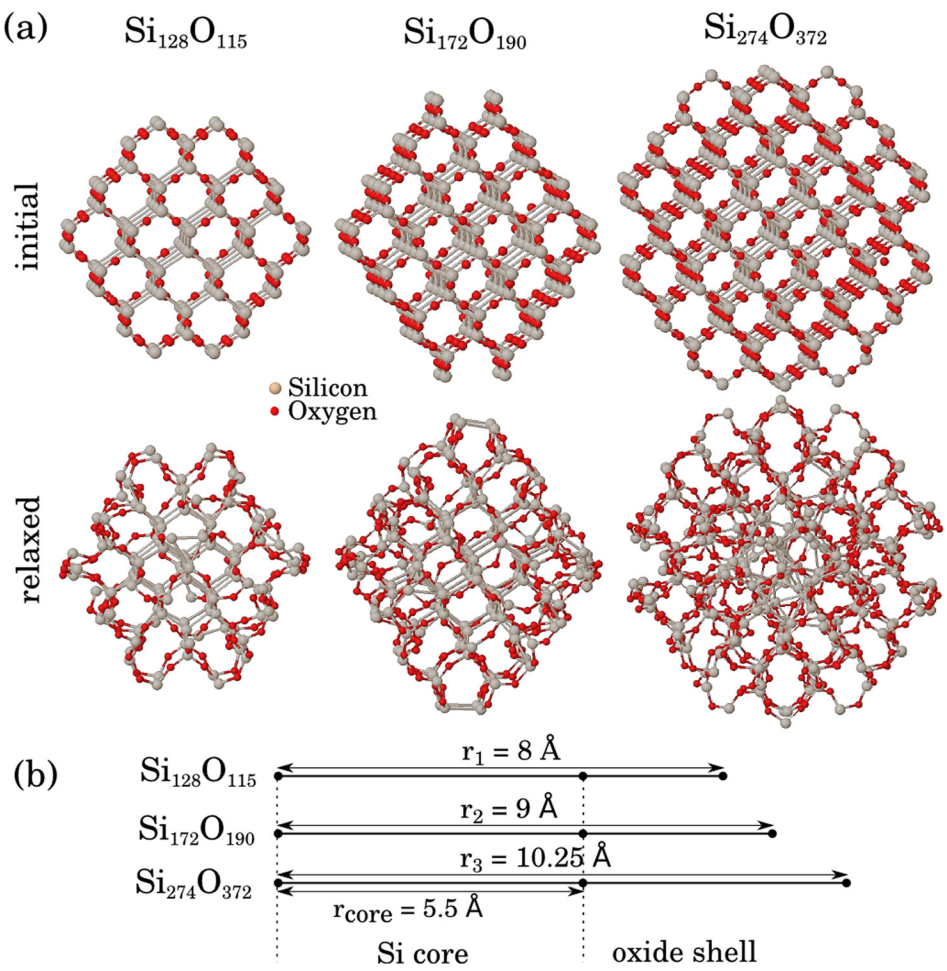

FIG. 1. (a) The $Si_{128}O_{115}$, $Si_{172}O_{190}$, and $Si_{274}O_{372}$ NCs before and after relaxation with CG calculations. (b) The silicon core diameter and oxide shell thickness in initial NCs. The silicon core diameter is 1.1 nm in all structures and the oxide shell thickness varies between 2.5 Å, 3.5 Å, and 4.75 Å.

$$\epsilon_1(\omega) - 1 = \frac{2}{\pi} \mathrm{P} \int_0^\infty \frac{\omega' \epsilon_2(\omega')}{\omega'^2 - \omega^2} d\omega', \tag{2}$$

where P denotes the principal value of the integral. Given the real and imaginary parts of the complex dielectric function, the extinction coefficient and thus the optical absorption coefficient can be evaluated.[52]

III. RESULTS AND DISCUSSION

A. Optical absorption coefficient

The calculated absorption coefficient spectrum is presented in Fig. 2(a). GGA-DFT while being suitable in trend prediction, is well-known to under-estimate the band-gap.[37,53,54] Thus, we focus on the trends which are in good agreement with available experimental data.

The optical absorption spectrum indicates that (i) the considered NCs show two major absorption peak sets: the smaller peaks between 0 and 2 eV and the intense broader peaks around ~5.5–6 eV, (ii) with increased shell thickness, the optical absorption coefficient is reduced and the absorption peak energy is red-shifted in the low-energy part of the spectrum which is more clearly observed in the imaginary part of dielectric function presented in Fig. 2(b). The origin of the observed peaks can be due to transitions of silicon, silica, intermediate suboxide species and defects at the Si-SiO_2 interface. Stress or trap levels, which will be discussed later, can affect the trends. The broad peak remarkably resembles the experimental absorption coefficient spectrum of SiO_2 (Ref. 55) which is added as the bold line in Fig. 2(a).

There are two low-energy maxima in the imaginary component of the dielectric function (Fig. 2(b)) which are similar to that of ϵ_2 spectral line-shape of silicon.[55,56] Thus, the low-energy peaks can be ascribed to the silicon suboxide species at the interface, which can reduce the optical gap through the creation of electrically active mid-gap trap levels. The peak intensities also depend on the oxide shell thickness. According to Fig. 2(a), the NC with thinnest oxide shell has the maximum absorption coefficient in the low energy part of optical absorption spectrum, whereas the NC with the thickest oxide shell has the maximum absorption coefficient in the high energy part of the spectrum. Similar trends are observed in the imaginary part of dielectric function (Fig. 2(b)). Thus, it can be inferred that the low (high) energy part of the optical response of core-shell Si-oxide NCs is mostly associated with silicon (oxygen) atoms, and the absorption strength is governed by the relative measure of the oxide shell thickness and the radius of the central silicon cluster. This trend is also observed in the electronic properties that will be discussed later in this work. Built-in interfacial stress, suboxide species of the transition region and the related dangling bonds can affect the electronic and optical properties of NCs.

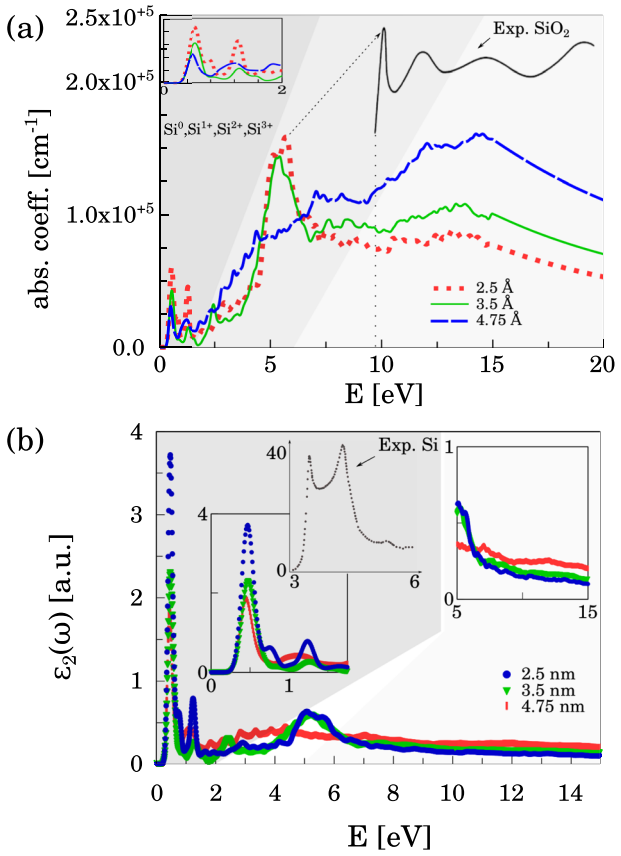

FIG. 2. (a) The calculated optical absorption coefficient spectrum for NCs with diameters of 1.6 nm, 1.8 nm, and 2.05 nm, and the experimental absorption coefficient spectrum of SiO_2 from Ref. 55. (b) The calculated imaginary part of dielectric function of considered NCs and the experimental data of silicon are taken from Refs. 55 and 56.

B. Structural effect of oxide shell

Despite numerous experimental attempts, a thorough understanding of the Si-SiO_2 interface is missing. However, it is generally accepted that two distinct regions can be identified: (i) the near-interface region which consists of a few atomic layers containing Si atoms in intermediate oxidation states. The experimental results range from atomically sharp to extended interfaces with a width of about 7 Å.[16,32,33,35,36] (ii) A second region which extends about 30 Å into SiO_2 overlayer. It is common to assume an atomically abrupt interface with a sub-oxide transition width of ∼2–3 Å for curved Si-SiO_2 interface.[26,27,35,36,38] In this work, NCs are defined with a capping shell thickness in the range of 2 Å–4.75 Å to accommodate the above-mentioned transition region width.

Fig. 3 depicts the NC cross-section before and after structural relaxation for a thin slice which passes through the center of NC. It is clearly seen that a considerable compressive stress is exerted on the embedded silicon NC as the oxide shell thickness increases. The results are in agreement with experimental data.[11,30,57–59] At the Si-SiO_2 interface, where two materials merge with a large density gradient (∼9%), deformations in both sides are created in order to accommodate the transition[60] that results in the observed compressive stress on the interior silicon NC.

The transition from Si to SiO_2 takes place through a highly disordered interfacial layer. The region containing different oxidation states of Si atoms, Si^{1+}, Si^{2+}, Si^{3+}, and Si^{4+}, with their nearest neighbor oxygen atoms constitute the interfacial layer. The distribution of silicon sub-oxide species versus their distance from the center of NC is plotted in Fig. 4. The results indicate that there is a relatively small number of oxidation states in the transition region that are concentrated close to the outermost Si layer, whereas a larger number of oxidation states spread over a broader region.

The root mean square (RMS) of the width of the transition region can be defined as $\sigma^2 \sum (r_i - \bar{r})^2 / N_{sub}$, where N_{sub} is the number of silicon sub-oxide species, and r_i is the distance of sub-oxide from the center of the NC, and $\bar{r} = \sum r_i / N_{sub}$ is the nominal position of the interface.[61–63] Accordingly, the calculated nominal position of the interface and the RMS width of the transition region for a center-passing rod with a radius of ∼2.5 Å are listed in Table I. By increasing the oxide shell thickness: (i) the nominal radius of the interface decreases ($\bar{r}$), (ii) the RMS width (σ) of the transition region increases, (iii) the number of higher (lower) oxidation states increases (decreases), and (iv) the sub-oxide species are pushed closer to the outermost Si layer and deeper into the shell.

According to Table I concentration variation of the five silicon chemical states is in good agreement with the experimental study of the as-deposited a-SiO_x films.[16] This indicates that as more oxygen becomes available more silicon atoms are oxidized into high oxidation states which leads to the reduction of Si^{1+} and Si^{2+} species concentration and the increase of high oxidation states. The results are also in agreement with the photo-emission evidences for flat Si-SiO_2 interfaces,[16,35,64] indicating that Si^{1+} and Si^{2+} species are mainly located at the interface and the Si^{3+} is distributed within a few Si-O bond lengths away from the interface.

The significant strain contrast is the source of the larger number of sub-oxides which corresponds to extended interface width. In addition, high oxidation states can reduce the band-gap of NC.[15] Thus, the identified increased number of high oxidation species is a cause of the observed slight red shift in the absorption spectrum. The increased number of sub-oxide species can affect the conduction and valence band tails, create trap levels, and modify the spatial distribution of the frontier molecular orbitals. A detailed investigation of the density of states and their spatial distribution is conducted next to elucidate the main factors governing the optical processes.

C. Partial and local density of states

To analyze the separated contribution of the core, interface, and shell atoms on the band-gap of considered NCs, the partial density of states (PDOS) is examined in Fig. 5. Several features are observed: (i) the density of states of core region remains constant in the three considered structures. And the density of states of either the silicon and the oxygen atoms increases with shell thickness with saving the line-shape, (ii) the conduction band (CB) and valence band (VB) tails shift as the shell thickness increases, which reduce the ground-state band-gap (see the inset of Fig. 5), and (iii) mid-

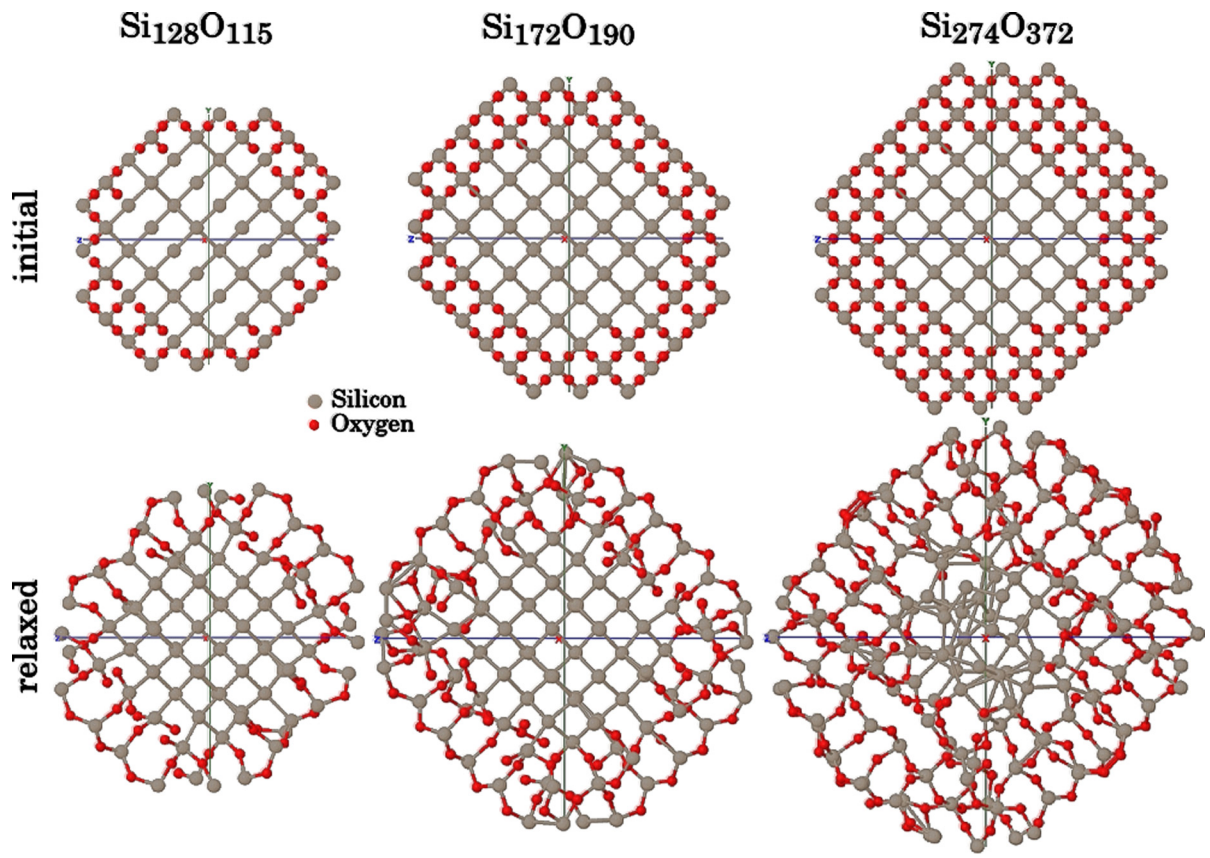

FIG. 3. The variations of silicon core diameter with oxide shell thickness for NCs with the same initial core diameter (1.1 nm) and varying oxide shell thicknesses (2.5 Å–4.75 Å). Cross sections are displayed for a thin slice which crosses the center of NCs before and after relaxation.

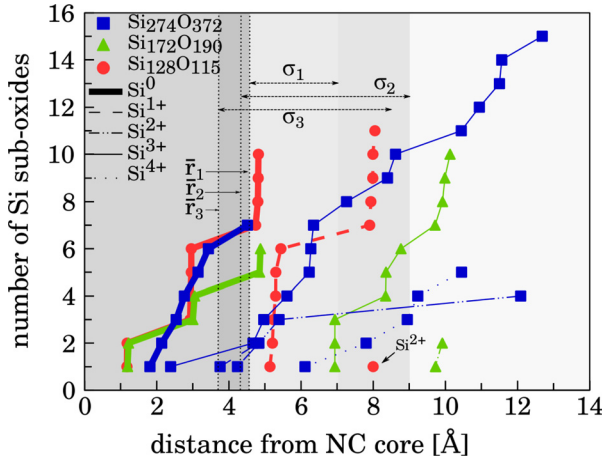

FIG. 4. The distribution of silicon sub-oxides as a function of their distance from the center of NC. σ denotes the rms width of the transition region, and $\bar{r}$ denotes the nominal radius of the core-shell interface. 1, 2, and 3 indices correspond to $Si_{128}O_{115}$, $Si_{172}O_{190}$, and $Si_{274}O_{372}$ NCs, respectively.

gap states appear in $Si_{274}O_{372}$ NC so that they nearly close the band-gap.

It is worth-mentioning that the ground-state HOMO-LUMO gap (electronic gap) which is depicted in the inset of Fig. 5(a) has a similar trend to that of the optical absorption peak variations which confirms the validity of the results. Part (ii) reveals the energy range where silicon and oxygen atoms mainly affect the band-gap of a core-shell Si-SiO_2 NC. The VB edge of the three discussed NCs shifts upward

TABLE I. The number of silicon sub-oxide species, the nominal radius of interface ($\bar{r}$), and the transition region width (σ) in a center-passing rod with a radius of ~ 2.5 Å for $Si_{128}O_{115}$, $Si_{172}O_{190}$, and $Si_{274}O_{372}$ NCs.

	Number of sub-oxides						
	Si^0	Si^{1+}	Si^{2+}	Si^{3+}	Si^{4+}	$\bar{r}$ (Å)	σ (Å)
$Si_{128}O_{115}$	10	11	1	0	0	4.700	2.353
$Si_{172}O_{190}$	6	0	2	10	1	4.440	4.602
$Si_{274}O_{372}$	7	2	4	15	5	3.761	4.717

with increased number of oxygen atoms which is in agreement with previous experimental studies on moderate oxidation of a bulk silicon samples.[34,65]

The percent-stacked chart of the oxygen and silicon atoms to the total DOS for $Si_{274}O_{372}$ NC in an energy window around the Fermi level is depicted in Fig. 6. Oxygen-induced states (interface + shell) mainly affect the valence band tails (light area bellow the Fermi level), whereas the silicon-related states (core + interface + shell) mainly affect the conduction band tail (dark area above the Fermi level), which is in accordance with the observed optical response that has been discussed earlier. These results are also in agreement with photo-emission experiments for a-Si films covered with oxygen mono-layers which indicate oxygen-induced variations in the valence band tail.[65] This can be interpreted through the large electro-negativity difference between the oxygen and the nearest-neighbor Si atom that

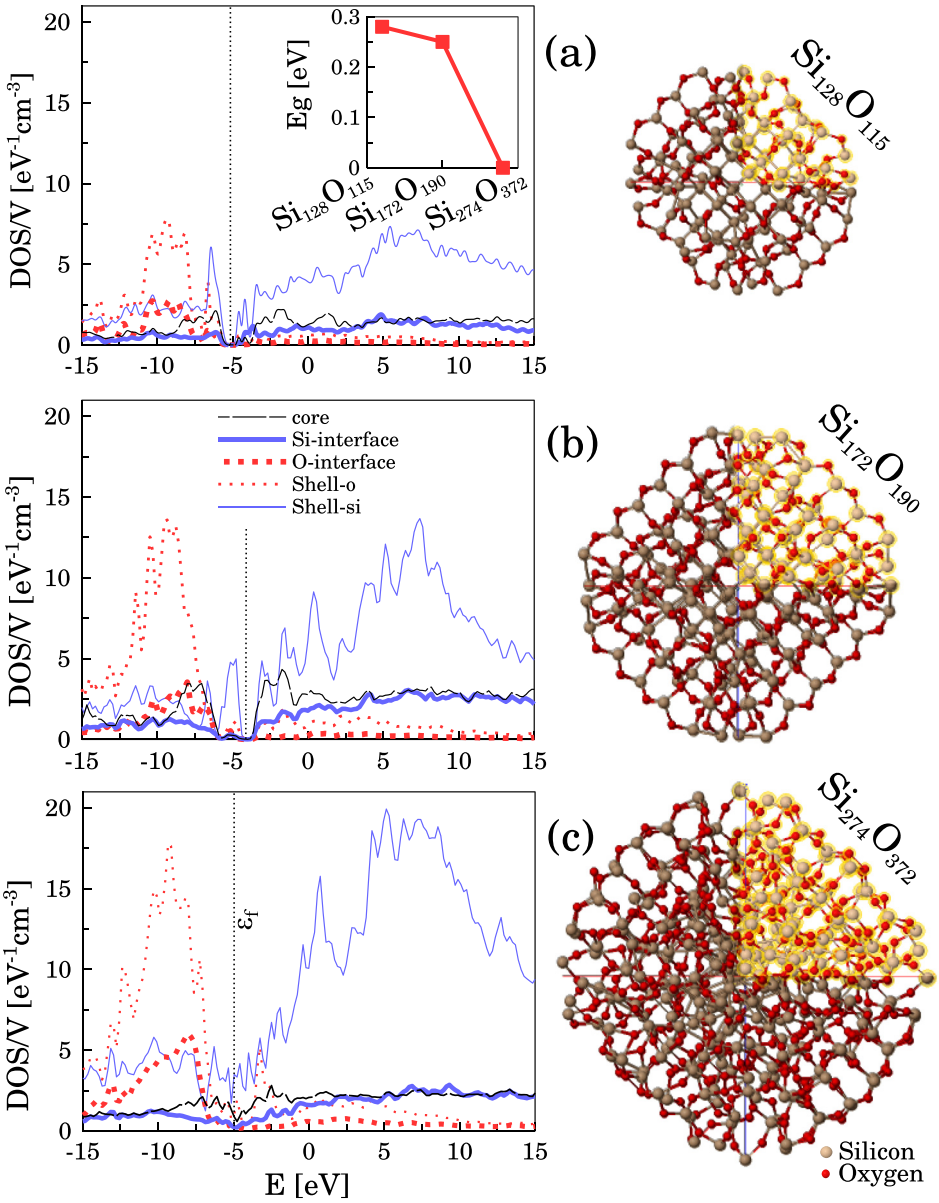

FIG. 5. Partial density of states of $Si_{128}O_{115}$, $Si_{172}O_{190}$, and $Si_{274}O_{372}$ NCs for silicon and oxygen atoms of core, interface, and shell regions. The inset shows the ground-state HOMO-LUMO band-gap variations.

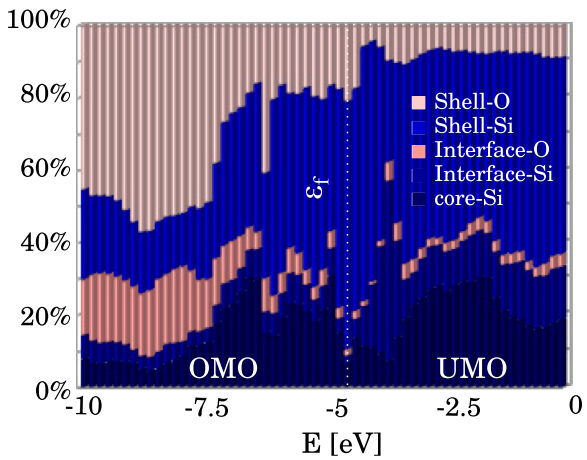

FIG. 6. The percent-stacked chart for the density of states of silicon and oxygen atoms for $Si_{274}O_{372}$ NC, separated for core, interface and shell regions. UMO (OMO) denotes the (un-)occupied molecular orbital. The light (dark) area corresponds to oxygen (silicon) atoms.

results in a transfer of charge density localization center from the neighboring Si sites to the oxygen and a consequent raising of the Si p and s levels. The VB tail states are mainly involved in the bonding or non-bonding O(2p) states, and the CB tail states are mostly formed from either a localized anti-bonding Si-O level or a CB state involving Si-Si and Si-O interactions.

In order to study the origin of the observed mid-gap states in part (iii) the spatial distribution of the density of HOMO and LUMO states is plotted in Fig. 7. Only in case of $Si_{274}O_{372}$, the HOMO density distribution involves a localized feature near the center of NC, which is absent in its LUMO distribution. Thus, the local density of states (LDOS)—as a comprehensive visual representation of eigenstates—is also examined with an energy window which involves the energy range consisted of larger number of frontier molecular orbitals. LDOS is by definition, the number of states per unit energy weighed by the spatial distribution of each state weighted by the Fermi energy[66]

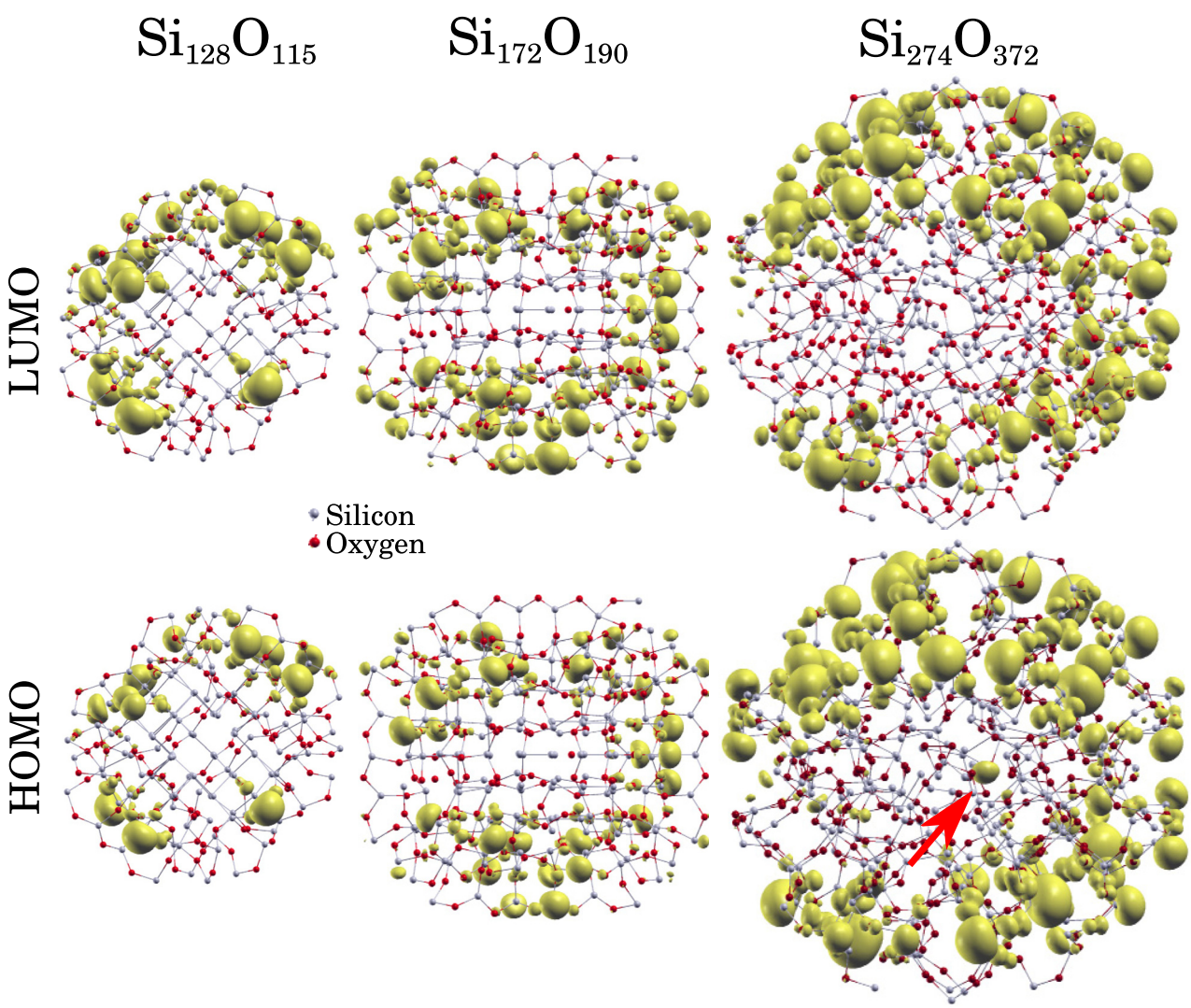

FIG. 7. The density iso-surfaces of HOMO and LUMO for $Si_{128}O_{115}$, $Si_{172}O_{190}$, and $Si_{274}O_{372}$ NCs with an iso-value of 0.004 electron/Å^3. Only positive polarity is plotted.

$$D(r;E) = 2\sum_n |\langle r|\phi_n\rangle|^2 \delta(E - E_n), \tag{3}$$

where the sum extends over both occupied and empty states. The interpretation of LDOS is similar to the constant current scanning tunneling microscope (STM) images which are the maps of constant LDOS close to the Fermi energy. The LDOS integrated in an energy window (± 0.1 eV) around the HOMO/LUMO energies is plotted in Fig. 8. The calculations are carried out using the SIESTA code[48] and the results are visualized by utilizing the XCrySDen software.[67] With increased shell thickness, both of the occupied and unoccupied frontier molecular orbitals partially migrate to the central silicon NC which is clearly observed in $Si_{274}O_{372}$. This is in contrast to the observed central feature of the density iso-surfaces of the HOMO state which is not observed in the LUMO state. This can be due to the contribution of other frontier molecular orbitals which correspond to the observed mid-gap energy levels.

Remembering that the smallest nominal interface radius is observed in $Si_{274}O_{372}$ along with the observed protrusion of sub-oxides into the central cluster and knowing that high oxidation states of silicon are known to localize the wavefunctions,[15] it can be inferred that the migration of frontier molecular orbitals into the central region is due to the protruded silicon sub-oxides. However, another intriguing explanation can be due to charge transfer from surface atoms as a result of surface relaxation effects and a consequent strengthening of their back-bonds which lead to the observed migrations. As a summary, the red shift in the optical gap and the corresponding reduction in the ground-state HOMO-LUMO gap are mainly because of the protrusion of sub-oxide species into the core silicon NC as a result of relaxing the excess strain exerted by the thick oxide shell.

IV. CONCLUSIONS

A comprehensive computational study using DFT of the effect of oxide shell thickness on the structural, optical, and electrical properties of Si-SiO_2 core-shell stand-alone NC is presented. The optical absorption spectrum of such NCs consists of the parts: the high energy section corresponds to the a-SiO_2 in which the peak energy is slightly blue shifted and the absorption strength is increased. The low energy section

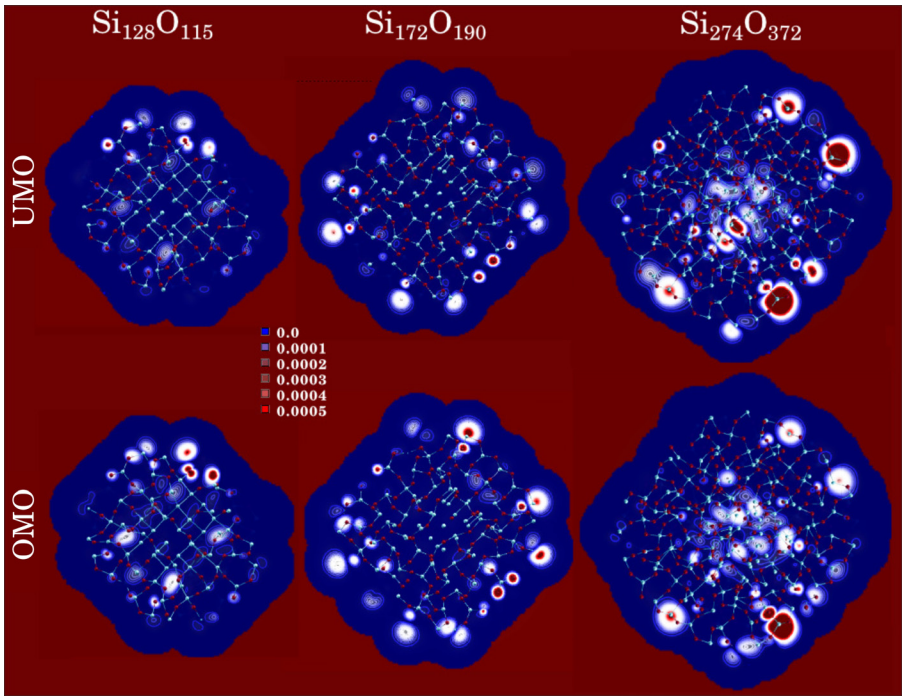

FIG. 8. The LDOS integrated in a ±0.1 eV energy window around HOMO and LUMO energies. The iso-energy contours are plotted for 0–0.0005 eV/bohr^3 iso-values.

corresponds to the silicon oxidation states in which the peak energy is slightly red shifted and the absorption strength is decreased. The percentage-resolved analysis of partial density of states indicates that the states in the valence band tail are mainly introduced by oxygen atoms and the states in the conduction band tail are mainly introduced by silicon atoms. Structural investigation demonstrates that a thicker oxide shell exerts larger compressive stress to the silicon core which affects the statistics and distribution of silicon sub-oxide species. Analysis of the distribution of sub-oxide species shows an increase (decrease) in the number of high (low) oxidation states, a decrease in the nominal radius of the interface, and an increased transition region width with the oxide shell thickness. Investigating the local density of states reveals the migration of frontier molecular orbitals into the central silicon cluster with increased shell thickness. Protrusion of sub-oxide species due to stronger stress from a thicker oxide shell can be viewed as misfit dislocations which correspondingly creates mid-gap trap levels which lead to the observed small red shift in the absorption peak energies of NCs.

ACKNOWLEDGMENTS

This work partly supported by Iran National Science Foundation (INSF) and the Iran Nanotechnology Initiative Council (INIC). The computational results presented have been achieved in part using the Vienna Scientific Cluster (VSC).

[1]H. Huff, *Into the Nano Era: Moore's Law Beyond Planar Silicon CMOS*, Springer Series Mate (Springer, Berlin Heidelberg, 2008).
[2]L. Brus, J. Phys. Chem. **90**, 2555 (1986).
[3]J. Derr, K. Dunn, D. Riabinina, F. Martin, M. Chaker, and F. Rosei, Physica E **41**, 668 (2009).
[4]V. Kumar, K. Saxena, and A. Shukla, IET Micro Nano Lett. **8**, 311 (2013).
[5]E. G. Barbagiovanni, D. J. Lockwood, P. J. Simpson, and L. V. Goncharova, J. Appl. Phys. **111**, 034307 (2012).
[6]J. R. Chen, D. C. Wang, H. C. Hao, and M. Lu, Appl. Phys. Lett. **104**, 061105 (2014).
[7]M. Kořínek, F. Trojánek, D. Hiller, S. Gutsch, M. Zacharias, and P. Malỳ, J. Appl. Phys. **117**, 093101 (2015).
[8]D. Kovalev and M. Fujii, Adv. Mater. **17**, 2531 (2005).
[9]M. Balaguer and E. Matveeva, J. Nanopart. Res. **12**, 2907 (2010).
[10]L. Canham, Appl. Phys. Lett. **57**, 1046 (1990).
[11]T. Arguirov, T. Mchedlidze, M. Kittler, R. Rölver, B. Berghoff, M. Först, and B. Spangenberg, Appl. Phys. Lett. **89**, 053111 (2006).
[12]C. M. Hessel, J. Wei, D. Reid, H. Fujii, M. C. Downer, and B. A. Korgel, J. Phys. Chem. Lett. **3**, 1089 (2012).
[13]R. Pereira, D. Rowe, R. Anthony, and U. Kortshagen, Phys. Rev. B **83**, 155327 (2011).
[14]J. A. L. López, J. C. López, D. V. Valerdi, G. G. Salgado, T. Díaz Becerril, A. P. Pedraza, and F. F. Gracia, Nanoscale Res. Lett. **7**, 604 (2012).
[15]X. Chen, X. Pi, and D. Yang, J. Phys. Chem. C **114**, 8774 (2010).
[16]W. Zhang, S. Zhang, Y. Liu, and T. Chen, J. Cryst. Growth **311**, 1296 (2009).
[17]F. Himpsel, F. McFeely, A. Taleb Ibrahimi, J. Yarmoff, and G. Hollinger, Phys. Rev. B **38**, 6084 (1988).
[18]A. Nurbawono, S. Liu, and C. Zhang, J. Chem. Phys. **142**, 154705 (2015).
[19]G. Seguini, C. Castro, S. Schamm Chardon, G. BenAssayag, P. Pellegrino, and M. Perego, Appl. Phys. Lett. **103**, 023103 (2013).
[20]A. Puzder, A. Williamson, J. C. Grossman, and G. Galli, Phys. Rev. Lett. **88**, 097401 (2002).
[21]P. Carrier, Phys. Rev. B **80**, 075319 (2009).
[22]E. W. Draeger, J. C. Grossman, A. J. Williamson, and G. Galli, J. Chem. Phys. **120**, 10807 (2004).
[23]Y. Shu and B. G. Levine, J. Phys. Chem. C **119**, 1737 (2015).
[24]S. Chopra and B. Rai, J. Nanostruct. Chem. **5**, 195 (2015).
[25]A. Puzder, A. Williamson, J. C. Grossman, and G. Galli, J. Chem. Phys. **117**, 6721 (2002).
[26]Z. Zhou, L. Brus, and R. Friesner, Nano Lett. **3**, 163 (2003).
[27]H. Dong, T. Hou, X. Sun, Y. Li, and S. T. Lee, Appl. Phys. Lett. **103**, 123115 (2013).
[28]P. Kroll and H. J. Schulte, Phys. Status Solidi B **243**, R47 (2006).
[29]M. Wolkin, J. Jorne, P. Fauchet, G. Allan, and C. Delerue, Phys. Rev. Lett. **82**, 197 (1999).
[30]T. Ye Liao, Z. Yu Hua, Z. Jun, X. Chun Lai, C. Bu Wen, W. Qi Ming, and X. Jun, Chin. Phys. B **21**, 077402 (2012).
[31]D. E. Yilmaz, C. Bulutay, and T. Çağin, Appl. Phys. Lett. **94**, 191914 (2009).
[32]F. Rochet, C. Poncey, G. Dufour, H. Roulet, C. Guillot, and F. Sirotti, J. Non-Cryst. Solids **216**, 148 (1997).
[33]J. Oh, H. Yeom, Y. Hagimoto, K. Ono, M. Oshima, N. Hirashita, M. Nywa, A. Toriumi, and A. Kakizaki, Phys. Rev. B **63**, 205310 (2001).

[34]P. Carrier, Z.-H. Lu, L. Lewis, and M. Dharma-wardana, Appl. Surf. Sci. **212**, 826 (2003).
[35]A. Pasquarello, M. S. Hybertsen, and R. Car, Appl. Surf. Sci. **104**, 317 (1996).
[36]N. Tit and M. Dharma Wardana, J. Appl. Phys. **86**, 387 (1999).
[37]A. J. Williamson, J. C. Grossman, R. Q. Hood, A. Puzder, and G. Galli, Phys. Rev. Lett. **89**, 196803 (2002).
[38]F. Djurabekova and K. Nordlund, Phys. Rev. B **77**, 115325 (2008).
[39]M. Luppi and S. Ossicini, Phys. Status Solidi A **197**, 251 (2003).
[40]Z. Huiwen, L. Yongsong, M. Lingfeng, S. Jingqin, Z. Zhiyan, and T. Weihua, J. Semicond. **31**, 082003 (2010).
[41]R. Guerra, I. Marri, R. Magri, L. Martin-Samos, O. Pulci, E. Degoli, and S. Ossicini, Phys. Rev. B **79**, 155320 (2009).
[42]N. A. Nama, M. A. Abdulsattar, and A. M. Abdolletif, J. Nanomater. **2010**, 952172.
[43]Y. Matsumoto, A. Dutt, G. Santana Rodríguez, J. Santoyo Salazar, and M. Aceves Mijares, Appl. Phys. Lett. **106**, 171912 (2015).
[44]N. Daldosso, M. Luppi, S. Ossicini, E. Degoli, R. Magri, G. Dalba, P. Fornasini, R. Grisenti, F. Rocca, L. Pavesi *et al.*, Phys. Rev. B **68**, 085327 (2003).
[45]T. J. Pennycook, G. Hadjisavvas, J. C. Idrobo, P. C. Kelires, and S. T. Pantelides, Phys. Rev. B **82**, 125310 (2010).
[46]G. H. Lu, M. Huang, M. Cuma, and F. Liu, Surf. Sci. **588**, 61 (2005).
[47]A. Puzder, A. Williamson, F. Reboredo, and G. Galli, Phys. Rev. Lett. **91**, 157405 (2003).
[48]J. M. Soler, E. Artacho, J. D. Gale, A. Garcia, J. Junquera, P. Ordejon, and D. Sanchez Portal, J. Phys.: Condens. Matter **14**, 2745 (2002).
[49]M. Fuchs and M. Scheffler, Comput. Phys. Commun. **119**, 67 (1999).
[50]E. J. Santos and E. Kaxiras, ACS Nano **7**, 10741 (2013).
[51]A. Piróth and J. Sólyom, *Fundamentals of the Physics of Solids: Volume II: Electronic Properties*, Fundamentals of the Physics of Solids (Springer, Berlin, Heidelberg, 2008).
[52]G. Nazir, A. Ahmad, M. F. Khan, and S. Tariq, Comput. Condens. Matter **4**, 32 (2015).
[53]V. Kocevski, O. Eriksson, and J. Rusz, Phys. Rev. B **87**, 245401 (2013).
[54]I. Vasiliev, S. Ögüt, and J. R. Chelikowsky, Phys. Rev. Lett. **86**, 1813 (2001).
[55]S. Pantelides, *Proceedings of the International Topical Conference on the Physics of SiO_2 and its Interfaces* (Elsevier, Yorktown Heights, New York, 1978).
[56]D. E. Aspnes and A. A. Studna, Phys. Rev. B **27**, 985 (1983).
[57]D. Yu, S. Lee, and G. S. Hwang, J. Appl. Phys. **102**, 084309 (2007).
[58]Z. Ma, X. Liao, G. Kong, and J. Chu, Appl. Phys. Lett. **75**, 1857 (1999).
[59]G. Zatryb, J. Misiewicz, P. Wilson, J. Wojcik, P. Mascher, and A. Podhorodecki, Thin Solid Films **571**, 18 (2014).
[60]G. Hadjisavvas and P. Kelires, Physica E **38**, 99 (2007).
[61]G. Hadjisavvas and P. Kelires, Phys. Rev. Lett. **93**, 226104 (2004).
[62]Y. Tu and J. Tersoff, Phys. Rev. Lett. **84**, 4393 (2000).
[63]Y. Tu and J. Tersoff, Phys. Rev. Lett. **89**, 086102 (2002).
[64]A. Bongiorno, A. Pasquarello, M. S. Hybertsen, and L. Feldman, Phys. Rev. Lett. **90**, 186101 (2003).
[65]A. K. Jain, L. Hong, and S. Pankanti, "Localized excitations in amorphous silicon alloys," Technical Report No. DE93001790 (Technical Information Center Oak Ridge Tennessee, 1987).
[66]E. Hasselbrink and B. Lundqvist, *Dynamics*, Handbook of Surface Science (Elsevier Science, 2008).
[67]A. Kokalj, Comput. Mater. Sci. **28**, 155 (2003).